15-2 NUMERICAL SIMULATIONS OF THE FORMATION OF MELTING-LAYER CLOUD

Kazuaki YASUNAGA[*1], Akihiro HASHIMOTO[2], and Masanori YOSHIZAKI[1]
[1]Institute of Observational Research for Global Change, JAMSTEC Yokosuka headquarters , Kanagawa, Japan
[2] Meteorological Research Institute, 1-1, Nagamine, Tsukuba, Ibaraki, Japan

1. Introduction

A number of previously published observational studies have reported the common occurrence of cloudy layers at around 5 km elevation within the tropics. Mapes and Zuidema (1996) analyzed radiosonde data obtained during the Tropical Ocean Global Atmosphere Coupled Ocean–Atmosphere Response Experiment (TOGA COARE) and discovered that cloudy layers indirectly inferred from relative humidity profiles commonly occur around the melting level (approximately 550 hPa). Sugimoto et al. (2000) used ground-based Mie scattering lidar to observe the vertical distribution of clouds at Jakarta, Indonesia, over a period of 2 years and found that the height of the cloud base has a notable maximum at an altitude of approximately 5 km, especially during the wet season. Yasunaga et al. (2003) identified a mid-level peak in the cloud vertical distribution from aircraft lidar data obtained during the NASA Pacific Exploratory Mission-Tropics B (PEM-Tropics B). Yasunaga et al. (2006) used cloud profiling radar and lidar to determine the frequency distribution of the base heights of cloudy layers with little (or no) falling condensate particles. The observed clouds have base heights predominantly in the range 4.5–6.5 km, and most of the clouds are less than 500 m in thickness. The occurrence of thin cloudy layers at the 0°C level is frequent, especially during the Madden-Julian Oscillation (MJO) active phase when the coverage of stratiform-type radar echoes is much greater than that of convective-type radar echoes.

Corresponding author address: Kazuaki Yasunaga, Institute of Observational Research for Global Change, JAMSTEC Yokosuka headquarters, 2-15, Natsushima-Cho, Yokosuka-city, Kanagawa, 237-0061, Japan: E-mail: yasunaga@jamstec.go.jp

Johnson et al. (1996) described prominent stable layers at heights of 2, 5, and 15–16 km observed during TOGA COARE. Johnson et al. (1999) also found that maxima in the vertical distributions of radar echo (cloud) tops occur in the vicinity of these three stable layer heights. Environmental static stability influences the vertical profiles of detrainment from cumulus convection as well as the top heights of cumulus convection (e.g., Bretherton and Smolarkiewicz 1989; Taylor and Baker 1991; Zuidema 1998; Mapes 2001; Takayabu et al. 2006). It has therefore been considered that the commonly observed mid-level cloud layers mainly originate via detrainment from cumulus convection that is promoted by the stable layer ("detrainment shelves" of Mapes and Zuidema 1996).

On the other hand, condensation can occur within a layer that contains melting ice particles because ice particles can melt within the regions of high relative humidity around 100% above the temperature of 0°C and melting diabatic cooling increases relative humidity. Rutledge and Hobbs (1983) used a numerical model to investigate the enhancement of precipitation in a “seeder-feeder” situation within warm-frontal rainbands. From the simulations, it was found that condensation occurs due to strong cooling associated with melting of snow from the seeder cloud and that the maximum cloud liquid water content in the feeder cloud is located just below the 0°C level. Stewart et al. (1984) took measurements from an aircraft flown through the melting layer of stratiform clouds over the California Valley and identified an isothermal layer at the 0°C level as well as large amount of cloud liquid water slightly below the 0°C level. It was inferred that the melting process within the stratiform precipitation region is possibly associated with the production of cloud liquid water

and consequent enhancement of precipitation. Szyrmer and Zawadzki (1999) used a numerical model to demonstrate that the non-uniformity of snow content causes horizontal variability in various atmospheric properties within the melting layer and that this in turn leads to the generation of convective cells. Consequently, the possibility exists that diabatic cooling due to the melting process might be responsible for the formation of mid-level thin cloud that is commonly observed in the tropics, especially the cloud at the 0°C level.

Yasunaga et al. (2006) showed that thin clouds and layers with high relative humidity appear just below the 0°C level several hours after stratiform precipitation becomes active. The stable layer does not predate the appearance of the layer with high relative humidity. In contrast, the enhanced stability layer is simultaneously observed with high relative humidity and is located just above the level of high relative humidity. Moreover, the weakened stability layer is also synchronously found below the level of high relative humidity. Melting diabatic cooling can account for the simultaneous appearance of layers with high relative humidity and enhanced and weakened stability layers (e.g., Stewart et al. 1984; Johnson et al. 1996). Therefore, Yasunaga et al. (2006) suggested that the cloudy layer (and the layer with high relative humidity) around the 0°C level is brought about by the melting process within the stratiform precipitation region rather than detrainment of surface-based convection; this type of cloud was named “melting-layer cloud.”

As described above, there are two candidate processes that are able to explain the common occurrence of cloudy layers around the 0°C level in the tropics: cloud detrainment promoted by the stable layer and enhanced condensation to compensate melting cooling. Although both processes are plausible, little attention has been paid to diabatic cooling associated with the melting process. Therefore, in the present study, we use a two-dimensional cloud-resolving model, and conduct numerical simulations of a squall-line in order to examine: (1) whether mid-level thin cloud is able to form within an environment without a stable layer, and (2) what causes the mid-level thin cloud to form, especially at the 0°C level—the presence of a stable layer or melting cooling.

2. Model descriptions and experimental design

Numerical simulations were performed using version 2.1 of the Weather Research and Forecasting (WRF) model, which solves fully compressible nonhydrostatic equations. The basic equations and a description of the numerics can be found in Skamarock et al. (2001) and Wicker and Skamarock (2002). A third-order-accurate Runge-Kutta scheme is used for the time integration. Fifth- and third-order schemes are utilized for spatial discretization in the horizontal and vertical directions, respectively. A 1.5-order scheme using a prognostic equation of turbulent kinetic energy (TKE) is applied to represent subgrid-scale effects (Klemp and Wilhelmson 1978). Cloud microphysical parameterization includes five categories of water condensates (cloud water, rainwater, cloud ice, snow, and graupel), and is based on Lin et al. (1983) and Rutledge and Hobbs (1984). Although the original code of the WRF model does not allow evaporation from rain, snow, and graupel at values of relative humidity above 90%, in the present study we modify the cap on evaporation to 100% relative humidity. Radiation and land-surface schemes are not employed in the present study.

The model domain is limited to two dimensions (horizontal and vertical). The horizontal grid size is 250 m with the domain covering an area of 500 km (2000 grid points). The model has 95 layers in the vertical and a top boundary at 24 km, corresponding to a grid size of about 250 m. The model employs the time-splitting method proposed by Klemp and Wilhelmson (1978). In the present study, the large time step is set to 3 s, with 6 small time steps within each large step. Rayleigh damping is imposed near the upper boundary, and open lateral boundary conditions are specified. The Coriolis parameter is set to zero.

Environmental conditions prior to the initiation of

convection are set to be horizontally homogeneous. While the sounding is based on a composite analysis by LeMone et al. (1994), some modifications are introduced. The original profile analyzed by LeMone et al. (1994) is used in the Global Energy and Water Cycle Experiment (GEWEX) Cloud System Study (GCSS) model intercomparisons, and is thought to be characteristic of the environment prior to the development of a squall-line (see Redelsperger et al. 2000, hereafter R2000). The profile of horizontal wind is shown in Fig. 1a. Low-level shear provides favorable conditions for the development of long lasting squall-lines (Rotunno et al. 1988). To eliminate the influence of fluctuations in humidity, temperature and horizontal wind profiles, we assume constant relative humidity (85%) above 2 km height (with respect to ice saturation below 0°C), a pseudo-adiabatic lapse rate between heights of 2 and 10 km (Fig. 1b), and constant vertical shear of horizontal wind above 2 km (Fig. 1a).

Deep convection is initiated in the numerical simulation by placing a 20 km surface-based cold temperature anomaly at time = 0. The 1.2 km-deep cold pool has temperature and moisture deficits of 3.5 K and 3.5 g kg^{-1} from the environmental sounding, respectively. To keep the convective system within the simulation domain, the model domain is translated at a constant speed of 12 m s^{-1} along the x direction. The model is integrated up to 17 hours (h).

3. Formation of melting-layer cloud in the numerical simulation

A cloudy grid box is defined as one in which the mixing ratio for those hydrometeors with small terminal velocity (cloud water, cloud ice, and snow) exceeds 0.05 g kg^{-1}. At the early stage of the squall-line, clouds reach a height of 15 km (Fig. 2a) with the cloud top height decreasing to 10 km at 5 h. Although the initial temperature profile does not show a mid-level stable layer (Fig. 1b), there is a notable peak in cloud coverage just below the 0°C level. If snow is excluded from the “cloud” variables, the peak in the middle level is still prominent (not shown), and does not depend on the “cloud” definition. Enhanced and weakened stability layers simultaneously appear above and below the peak level of cloud coverage (Fig. 2b), which is in agreement with the situation where melting-layer cloud was observed (Yasunaga et al. 2006). As most of the two-dimensional experiments in R2000 show a maximum in total hydrometeor content at the melting level (e.g., Fig. 17 in R2000), mid-level thin cloud would be robust regardless of the chosen models.

To clarify the process responsible for the mid-level thin cloud observed in Fig. 2a, changes in the cloud mixing ratio due to dynamic process (advection and diffusion) and cloud microphysics (condensation, evaporation, coalescence, aggregation, riming, etc.) are averaged over the model domain for a 17-hour period (Fig. 3). As the majority of condensates associated with the squall-line remain within the computational domain at 17 h, the domain-averaged changes of condensates by dynamic process in Fig. 3 result from vertical advection and vertical diffusion.

Although both profiles of the change in the cloud mixing ratio have a pronounced maximum around the height of 5 km (Fig. 3), the peak level of cloud microphysics is closer to the peak level of cloud coverage (Fig. 2a). In addition, the peak value of cloud microphysics is much greater than that of the dynamic process. Therefore, it can be said that cloud microphysics is responsible for the occurrence of mid-level thin cloud.

While the mid-level thin cloud is associated with cloud microphysics, total diabatic heating via cloud microphysics shows no notable peak around the height of 5 km (Fig. 4a); however, intense heating associated with the vapor-liquid or vapor-ice phase change occurs at the 0°C level, which approximately balances the strong melting cooling. The approximate balance between condensation or sublimation heating and melting cooling is locally maintained (not shown).

In the convective region near the leading edge (395–450 km), condensation or sublimation heating is the main contributor to the total diabatic heating (Fig. 4b). In the rear region of the squall-line (300–395 km),

melting cooling and condensation or sublimation heating are approximately canceled, while total heating shows a typical profile of the stratiform region and no notable feature at the 0°C level (Fig. 4c). Therefore, the mid-level thin cloud is formed in the rear region of the squall-line.

It is possible that the enhanced condensation or sublimation is the cause of the intensified melting cooling. Condensation heating is, however, much larger than sublimation heating at the 0°C level, and the heating due to the phase change from liquid to ice above the 0°C level is much smaller than the cooling from ice to liquid in Fig. 4. In addition, the intensified melting cooling should be located in the rear of the enhanced condensation heating, if ice formation following the enhanced condensation intensifies melting cooling. The condensation heating region, however, coincides with the melting cooling region, and the approximate balance is locally attained. The coincident location indicates that strong melting cooling is the cause of the enhanced condensation at the 0°C level. In other words, ice formation following the enhanced condensation does not produce a notable peak of melting cooling at the 0°C level, but melting cooling enhances condensation. The simulated mid-level thin cloud is the “melting-layer cloud” suggested by Yasunaga et al. (2006).

Figure 5 represents the evolution of the simulated squall-line from 6 to 10 h at 30 minute intervals. The domain is subjectively partitioned into three regions (R1, R2, and R3), according to the stage of convective cells. At 6 h, active convective cells develop in the leading region of the squall-line (R1 in Fig. 5a), mature at 7 h (R2 in Fig. 5c), and gradually decay after 7 h and 30 min (R2 in Figs. 5d and 5e, and R3 in Figs. 5f and 5g). After the development of several weaker convective cells from 7 to 8 h near the leading edge of the squall-line (R1 in Figs. 5c, 5d and 5e), even more vigorous convective cells appear at 8 h and 30 min (R1 in Fig. 5f), and reach the height of 15 km at 10 h (R2 in Fig. 5i). In the trailing part of the active convective cells which develop from 6 h, thin cloud is found around 5 km at 8 h and 30 min (R3 in Fig. 5f), is left behind from the front part of the convective cells at 9 h (R3 in Fig. 5e), and then, is overlapped by the following weaker convective cells at 9 h and 30 min and 10 h (R3 in Figs. 5h and 5i).

Figure 6 shows condensation rate profiles averaged over each region in Fig. 5 from 6 to 10 h at 30 minute intervals. In the leading region of the squall-line (R1), condensation occurs most vigorously, and the peak of the condensation rate is located around the height of 2–3 km. In the rear region of the squall-line (R2 and R3), the condensation peak is prominent at the height of 5 km (around the 0°C level). Although mid-level thin cloud is not identified in the R2 region of Fig. 5, condensation is pronouncedly enhanced at the height of 5 km within the R2 region, even when convective cells mature in the R2 region (e.g., Figs. 5c, 5i, 6c, and 6i).

References

Bretherton, C. S., and P.K. Smolarkiewicz, 1989: Gravity waves, compensating subsidence and detrainment around cumulus clouds, *J. Atmos. Sci.*, **46**, 740-759.

Johnson, R.H., P.E. Ciesielski, and K.A. Hart, 1996: Tropical inversions near the 0°C level, *J. Atmos. Sci.*, **53**, 1838-1855.

-, T. M. Rickenbach, S. A. Rutledge, P. E. Ciesielski, and W. H. Schubert, 1999: Trimodal characteristics of tropical convection, *J. Climate*, **12**, 2397-2418.

Klemp, J. B., and R. B. Wilhelmson, 1978: The simulation of three dimensional convective storm dynamics, *J. Atmos. Sci.*, **35**, 1070-1096.

LeMone, M. A., D. P. Jorgensen, and B. F. Smull, 1994: The impact of two convective systems of sea-surface stresses in COARE. Preprints, *6th Conference on Mesoscale Processes*, Amer. Meteor. Soc., Portland, 40-44.

Lin, Y.-L., R. D. Farley, and H. D. Orville, 1983: Bulk parameterization of the snow field in a cloud model. *J. Appl. Meteor.*, **22**, 1065–1092.

Mapes, B. E., and P. Zuidema, 1996: Radiative-dynamical consequences of dry tongues in the tropical troposphere, *J. Atmos. Sci.*, **53**,

620-638.

-, 2001: Water's two height scales: the moist adiabat and the radiative troposphere, *Q. J. R. Meteor. Soc.*, **127**, 2353-2366.

Redelsperger, J. L., P. R. A. Brown, R. Guichard, C. Hoff, M. Kawasima, S. Lang, Th. Montmerle, K. Nakamura, K. Saito, C. Seman, W.K. Tao, and L.J. Donner, 2000: A GCSS model intercomparison for a tropical squall line observed during TOGA-COARE. Part I: Cloud-resolving models, *Q. J. R. Meteor. Soc.*, 126, 823-863.

Rotunno, R., J. B. Klemp, and M. L. Weisman, 1988: A theory for strong, long-lived squall lines, *J. Atmos. Sci.*, **45**, 463-485.

Rutledge, S. A., and P. V. Hobbs, 1983: The mesoscale and microscale structure and organization of cloud and precipitation in midlatitude cyclones. VIII: A model for the “Seeder-Feeder” process in warm-frontal rainbands, *J. Atmos. Sci.*, **40**, 1185-1206.

-, and -, 1984: The Mesoscale and microscale structure and organization of clouds and precipitation in midlatitude cyclones. XII: A diagnostic modeling study of precipitation development in narrow cold-frontal rainbands. *J. Atmos. Sci.*, **41**, 2949–2972.

Skamarock, W. C., J. B. Klemp, and J. Dudhia, 2001: Prototypes for the WRF (Weather Research and Forecasting) model. Preprints, *9th Conf. on Mesoscale Processes*, Fort Lauderdale, FL, Amer. Meteor. Soc., J11-J15.

Stewart, R. E., J. D. Marwitz, J. C. Pace, R. E. Carbone, 1984: Characteristics through the melting layer of stratiform clouds, *J. Atmos. Sci.*, **41**, 3227-3237

Sugimoto, N., I. Matsui, A. Shimizu, M. Pinandito, S. Sugondo, 2000: Climatological characteristics of cloud distribution and planetary boundary layer structure in Jakarta, Indonesia revealed by lidar observation, *Geophys. Res. Lett.*, 27(18), 2909-2912, 10.1029/2000GL011544.

Szyrmer, W., and I. Zawadzki, 1999: Modeling of the melting layer. Part I: Dynamics and microphysics, *J. Atmos. Sci.*, **56**, 3573-3592.

Takayabu, Y. N., J. Yokomori, and K. Yoneyama, 2006: A diagnostic study on interactions between atmospheric thermodynamic structure and cumulus convection over the tropical western Pacific Ocean and over the Indochina peninsula. *J. Meteor. Soc. Japan*, 84A, 151-169.

Taylor, G.R., and M.B. Baker, 1991: Entrainment and detrainment in cumulus clouds, *J. Atmos. Sci.*, **48**, 112-121.

Wicker, L. J., and W. C. Skamarock, 2002: Time splitting methods for elastic models using forward time schemes. *Mon. Wea. Rev.*, **130**, 2088-2097.

Yasunaga, K., H.Kida, and T. Satomura, 2003: The 600-750 hPa relative humidity minimum observed during PEM-Tropics B, *Geophysical Research Letters*, 30(24), 2282, doi: 10.1029/2003GL018739.

-, -, -, and N. Nishi, 2004: A Numerical Study on the Detrainment of Tracers by Cumulus Convection in TOGA COARE, *J. Meteor. Soc. Japan,* **82**, pp861-878.

-, K., K. Yoneyama, H. Kubota, H. Okamoto, A. Shimizu, H. Kumagai, M. Katsumata, N. Sugimoto, and I. Matsui, 2006: Melting-layer cloud observed during MR01-K05 cruise of Res/V Mirai, *J. Atmos. Sci.*, in printing.

Zuidema, P., 1998: The 600-800-mb minimum in tropical cloudiness observed during TOGA COARE, *J. Atmos. Sci.*, **55**, 2220-2228.

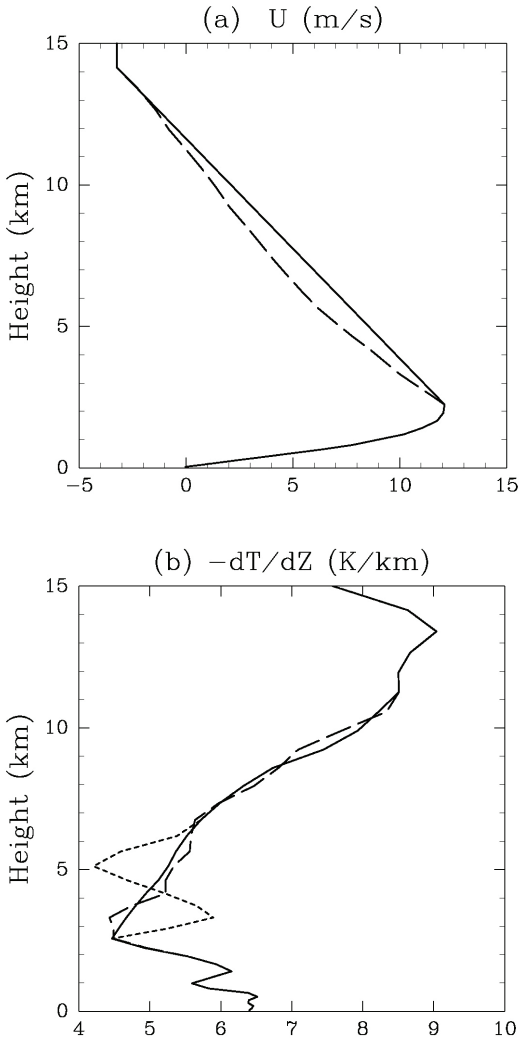

Fig. 1: (a) Initial profile of the horizontal wind (solid line). (b) Lapse rate calculated from initial temperature profile (solid line). Dashed lines in (a) and (b) represent the original profiles analyzed by LeMone et al. (1994). Dotted line in (b) indicates lapse rate calculated from initial temperature profile used in the sensitivity test (see Section 4a).

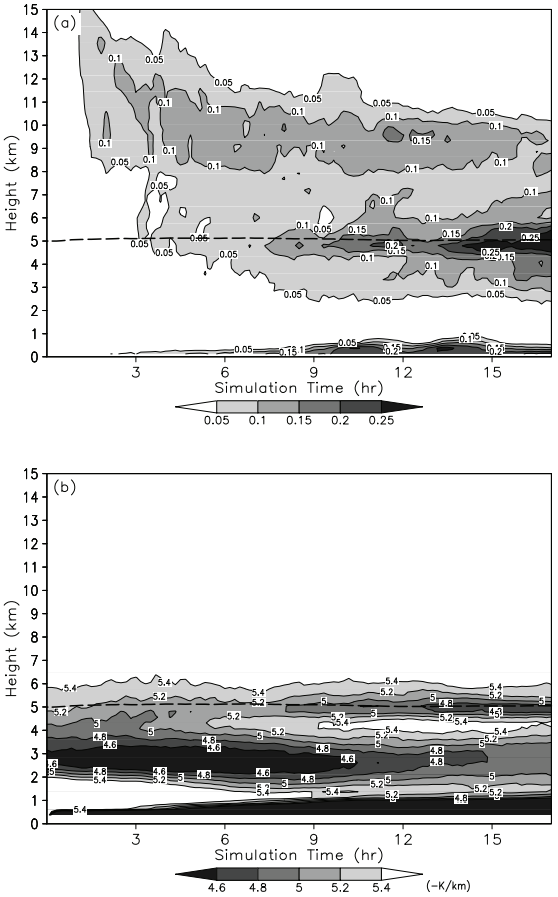

Fig. 2: Temporal record of vertical profiles of cloud fraction (a) and temperature lapse rate averaged over the model domain (b). A dashed line in each panel indicates the 0°C level.

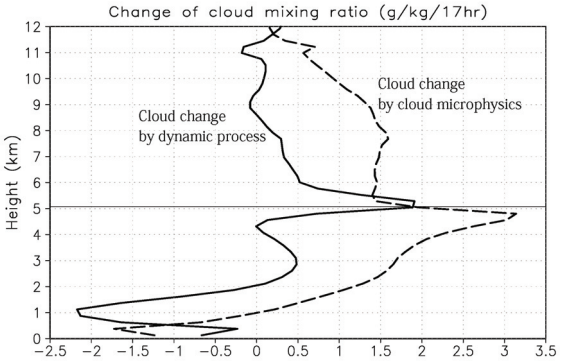

Fig. 3: Vertical profile of domain-averaged changes in the cloud (cloud water + cloud ice + snow) mixing ratio due to dynamic process (solid line) and cloud microphysics (dashed line) during the 17–hour period of the simulation.

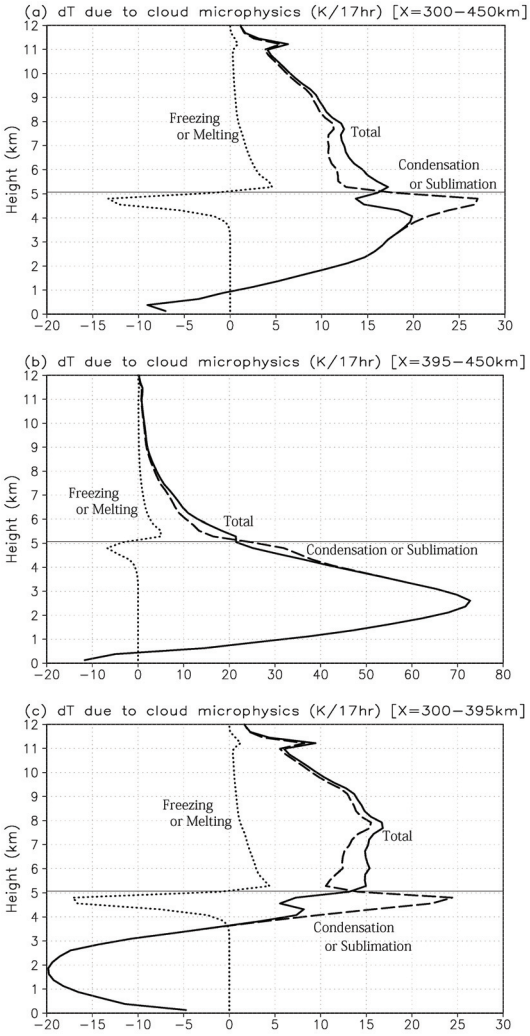

Fig. 4: Vertical profile of diabatic heating associated with cloud microphysics averaged over 300–450 km (a), 395–450 km (b), and 300–395 km (c) of the model domain. A solid line indicates total heating. Dashed and dotted lines represent heating due to phase changes between vapor and condensates (liquid or ice), and between liquid and ice, respectively.

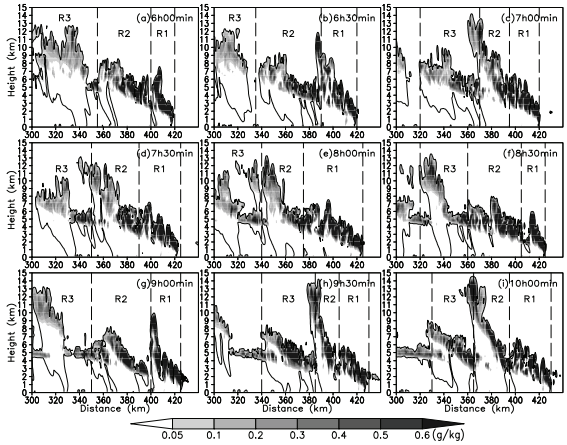

Fig. 5: Vertical cross sections of the cloud (cloud water + cloud ice + snow) mixing ratio from 6 to 10 h at 30 minute intervals. Contoured area represents the area exceeding the total hydrometeor of 0.05 g kg^{-1}. Only part of the simulation domain is shown.

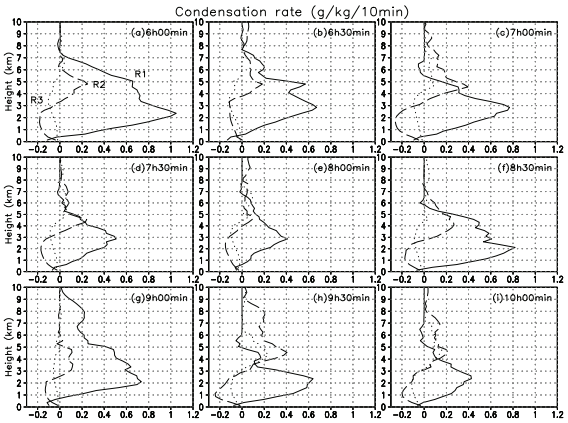

Fig. 6: Vertical profiles of condensation rate from 6 to 10h at 30 minute intervals. Solid, dashed, and dotted lines represent profiles averaged over R1, R2, and R3 regions in Fig. 5 during 10 minutes, respectively.